

# The First Moments of Nucleon Generalized Parton Distributions

P. Wang<sup>a,b,c</sup> and A. W. Thomas<sup>d</sup>

<sup>a</sup>*Institute of High Energy Physics, Chinese Academy of Science, Beijing 100049, P. R. China*

<sup>b</sup>*Theoretical Physical Center for Science Facilities (TPCSF), CAS, Beijing 100049, P. R. China*

<sup>c</sup>*Jefferson Laboratory, 12000 Jefferson Ave., Newport News, VA 23606 USA and*

<sup>d</sup>*CSSM, School of Chemistry and Physics, University of Adelaide, Adelaide SA 5005, Australia*

We extrapolate the first moments of the generalized parton distributions using heavy baryon chiral perturbation theory. The calculation is based on the one loop level with the finite range regularization. The description of the lattice data is satisfactory and the extrapolated moments at physical pion mass are consistent with the results obtained with dimensional regularization, although the extrapolation in the momentum transfer to  $t = 0$  does show sensitivity to form factor effects which lie outside the realm of chiral perturbation theory. We discuss the significance of the results in the light of modern experiments as well as QCD inspired models.

## I. INTRODUCTION

The study of hadron structure and, in particular, the spin structure of the proton is one of the most exciting challenges facing modern nuclear and particle physics. Through measurements of high energy scattering of electroweak probes one can measure the parton distribution functions (PDFs), which describe the number densities of partons with momentum fraction,  $x$ , in the nucleon. The study of the spin and flavor dependence of the PDFs has provided a wealth of data which has proven critical to our understanding of the structure of the nucleon [1].

In recent years, the extension of this concept to so-called generalized parton distributions (GPDs) has attracted enormous interest [2, 3]. The GPDs are related to the amplitude for deeply virtual Compton scattering where the initial and final photons have different momenta. It is widely anticipated that the GPDs should provide even more information concerning the internal structure of the nucleon. Of particular relevance to our present work is the link between the low moments of the GPDs and the angular momentum carried by each quark flavor within the proton [4]. This is now widely considered essential to a satisfactory resolution of the famous proton spin crisis [5, 6], because successful models suggest that a great deal of the proton spin is carried as quark orbital angular momentum [7–9].

There have been many theoretical and experimental studies of the GPDs. On the theoretical side, much of the work has centered on the most effect ways to parameterize them [10]. There has also been quite a bit of work on phenomenological models, such as the MIT and cloudy bag model [11, 12], the constituent quark model [13, 14], the NJL model [15], the light-front model [16, 17], the color glass condensate model [18] and the Bethe-Salpeter approach [19, 20]. On the experimental side, various groups have focussed on different kinematic ranges. ZEUS and H1 measured the DVCS cross section for the first time, with  $x_B$  in the very low range  $10^{-4} < x_B < 0.02$  [21, 22]. COMPASS focussed on a little larger  $x_B$  – from  $\simeq 0.01$  to  $\simeq 0.1$  [23]. The data from HERMES is in the range  $0.03 < x_B < 0.35$  [24, 25]. The study of the high  $x_B$  domain, where valence quarks should dominate, requires high luminosity and a high energy electron beam. With the JLab 12 GeV upgrade,  $x_B$  will range up to 0.7, while the current JLab data is in the range  $0.15 < x_B < 0.55$  [26–28].

The GPDs have a close relationship with the form factors. By integrating the GPDs with different powers of the momentum fraction  $x$ , the GPDs can be transformed into Mellin moments. There has been important work on the moments and form factors from various lattice QCD collaborations [29–31], as well as chiral perturbation theory [35–37]. As for many other observables computed in lattice QCD, current lattice simulations have been concentrated at quite large pion mass. While chiral perturbation theory is only expected to be convergent at quite low pion mass [33, 34], in order to relate the simulations at large quark mass to experimental data, the lattice data has been extrapolated using covariant and heavy baryon chiral perturbation theory with dimensional regularization – e.g., in Ref. [29].

Based on the observation that *all* hadron properties show a slow, smooth variation with quark mass above  $m_\pi \sim 0.4\text{GeV}$ , suggesting that chiral corrections (pion loops) are strongly suppressed there [32], an alternative regularization method, namely finite-range-regularization (FRR) has also been used to extrapolate the lattice data. It was first applied in the extrapolation of nucleon mass and magnetic moment [38–40]. The remarkably improved convergence properties of the FRR expansion mean that lattice data at large pion mass can be described very well and the obtained nucleon mass at physical pion mass is close to the experimental value. Later, the FRR method was applied to extrapolate the vector meson mass, nucleon magnetic moments, form factors, charge radii and strange form factors [41–48]. Finally, we note that FRR has the unique advantage that it provides a natural connection between physical results and quenched lattice data [41, 42, 45, 46].

In this paper, we will focus on the low moments of the GPDs. The LHPC lattice data will be used as input for

the extrapolation. The contribution from the disconnected quark loops has not been included in the lattice QCD simulation, which means that part of the sea quark contribution has been omitted [29]. While this contribution cancels in the isovector moments it could be very important in the isoscalar moments. Extensive investigation of other nucleon properties suggests that this omission might be more important at the physical quark mass than at the relatively heavy masses where the lattice calculations were made [32]. If this were the case, the chiral extrapolation, which *does* include contributions from disconnected diagrams, may yield a reasonable representation of the physical values, even for isoscalar quantities. This is indeed the case for the octet magnetic moments [47, 49], for example. On the other hand, we are unable to quantify the error associated with this procedure for isoscalar quantities and in future it would clearly be preferable to be able to work with lattice simulations which include the disconnected contributions.

The paper is organized as follows. In section II, we briefly introduce the chiral Lagrangian which is used for the calculation of the first moments. The first isovector and isoscalar moments will be derived in section III. Numerical results are presented in section IV and finally section V presents a summary of the results with some discussion.

## II. CHIRAL LAGRANGIAN

The generalized parton distribution functions,  $H^q(x, \xi, t)$  and  $E^q(x, \xi, t)$ , are defined as

$$\int \frac{d\lambda}{2\pi} e^{i\lambda x} \langle p', s' | \psi \left( -\frac{\lambda n}{2} \right) \not{n} \psi \left( \frac{\lambda n}{2} \right) | p, s \rangle = H^q(x, \xi, t) \bar{u}(p', s') \not{n} u(p, s) + E^q(x, \xi, t) \bar{u}(p', s') \frac{i\sigma^{\mu\nu} n_\mu Q_\nu}{2M_N} u(p, s), \quad (1)$$

where  $Q = p' - p$ ,  $t = Q^2$ ,  $\xi = -\frac{1}{2}n \cdot Q$  with  $n$  the light-like vector satisfying  $n^2 = 0$ ,  $\frac{1}{2}n \cdot Q = 1$ . These GPDs can be transformed into Mellin moments/form factors by integrating with different powers of the momentum fraction,  $x$ . The zero-th order moments correspond to the Dirac and Pauli form factors as

$$\int_{-1}^1 dx x^0 H^q(x, \xi, t) = F_1^q(t), \quad (2)$$

$$\int_{-1}^1 dx x^0 E^q(x, \xi, t) = F_2^q(t). \quad (3)$$

The Dirac and Pauli as well as the electric and magnetic form factors have been discussed widely in the literature. In this paper, we focus on the first moments of the nucleon GPDs:

$$\int_{-1}^1 dx x H^q(x, \xi, t) = A_{2,0}^q(t) + (-2\xi)^2 C_{2,0}^q(t), \quad (4)$$

$$\int_{-1}^1 dx x E^q(x, \xi, t) = B_{2,0}^q(t) - (-2\xi)^2 C_{2,0}^q(t). \quad (5)$$

The form factors  $A$ ,  $B$  and  $C$  can be calculated with the following equation:

$$i \langle p' | \bar{q} \gamma_{\{\mu} \overleftrightarrow{D}_{\nu\}} q | p \rangle = u(p') \left[ A_{2,0}^q(Q^2) \gamma_{\{\mu} \bar{p}_{\nu\}} - \frac{B_{2,0}^q(Q^2)}{2M_N} Q^\alpha i\sigma_{\alpha\{\mu} \bar{p}_{\nu\}} + \frac{C_{2,0}^q(Q^2)}{M_N} Q_{\{\mu} Q_{\nu\}} \right] u(p), \quad (6)$$

where the bracket,  $\{\dots\}$ , denotes the symmetrized and traceless combination of all indices in the operator.  $M_N$  is the nucleon mass and  $\bar{p}$  is the sum of the initial and final momenta. As one can see from the above equation, the first moments of the GPDs can be calculated by inserting into the nucleon states a tensor current which interacts with the external tensor field.

It is convenient to define the isospin scalar and vector form factors  $X$  ( $X=A, B$  or  $C$ ) with the combination of each quark's contribution:

$$X_{2,0}^{u+d}(Q^2) = X_{2,0}^u(Q^2) + X_{2,0}^d(Q^2), \quad (7)$$

$$X_{2,0}^{u-d}(Q^2) = X_{2,0}^u(Q^2) - X_{2,0}^d(Q^2). \quad (8)$$

In chiral perturbation theory, the interaction between tensor current and the external tensor field as well as the baryon-meson interaction can be written in a series of powers of momentum of the tensor and meson fields [35]. The lowest order Lagrangian is

$$\begin{aligned} \mathcal{L}^{(0)} = & \frac{1}{2} \bar{\psi}_N \left\{ i \left[ \frac{a_{2,0}^v}{2} u^\dagger V_{\mu\nu}^3 \tau^3 u + \frac{a_{2,0}^v}{2} u V_{\mu\nu}^3 \tau^3 u^\dagger + \frac{\Delta a_{2,0}^v}{2} u^\dagger V_{\mu\nu}^3 \tau^3 u \gamma_5 \right. \right. \\ & \left. \left. - \frac{\Delta a_{2,0}^v}{2} u V_{\mu\nu}^3 \tau^3 u^\dagger \gamma_5 + a_{2,0}^s V_{\mu\nu}^0 \right] \gamma^{\{\mu} \overleftrightarrow{D}^{\nu\}} \right\} \psi_N, \end{aligned} \quad (9)$$

where  $V_{\mu\nu}^i$  and  $V_{\mu\nu}^0$  are the isovector and isoscalar tensor fields. The covariant derivative  $\overleftrightarrow{D}^\mu$  is defined as  $\overleftrightarrow{D}^\mu = \overrightarrow{D}^\mu - \overleftarrow{D}^\mu$ , where  $\overrightarrow{D}^\mu = D^\mu = \partial^\mu + \frac{1}{2} [u^\dagger, \partial^\mu u]$ .  $U = u^2$  is the non-linear realization of the Goldstone boson field. As in Ref. [35], the parity-odd tensor interaction term is also included. In the above equation,  $\Delta a_{2,0}^v$  is only poorly known and it is related to the spin-dependent analogue of the mean momentum fraction, namely  $\langle \Delta x \rangle_{u-d}$ .

The  $\mathcal{O}(p^1)$  part of the interaction Lagrangian is expressed as

$$\begin{aligned} \mathcal{L}^{(1)} = & \bar{\psi}_N \left\{ i \gamma^\mu D_\mu - M_N + \frac{gA}{2} \gamma^\mu \gamma_5 u_\mu + \left( \frac{ib_{2,0}^v}{8M_N} [D_\alpha, u^\dagger V_{\mu\nu}^3 \tau^3 u + u V_{\mu\nu}^3 \tau^3 u^\dagger] \sigma^{\alpha\{\mu} D^{\nu\}} + h.c. \right) \right. \\ & \left. + \left( \frac{ib_{2,0}^s}{4M_N} [\partial_\alpha, V_{\mu\nu}^0] \sigma^{\alpha\{\mu} D^{\nu\}} + h.c. \right) \right\} \psi_N, \end{aligned} \quad (10)$$

where  $u_\mu$  is defined as  $u_\mu = iu^\dagger \partial_\mu u^\dagger$ . The  $\mathcal{O}(p^2)$  part of the interaction can be written as

$$\begin{aligned} \mathcal{L}^{(2)} = & F_\pi^2 T_r \left[ \partial^{\{\mu} U^\dagger \partial^{\nu\}} U x_\pi^0 V_{\mu\nu}^0 \right] - \frac{c_{2,0}^v}{2M_N} \bar{\psi}_N \left[ D^{\{\mu}, [D^{\nu\}}, u^\dagger V_{\mu\nu}^3 \tau^3 u + u V_{\mu\nu}^3 \tau^3 u^\dagger \right] \psi_N \\ & - \frac{c_{2,0}^s}{M_N} \bar{\psi}_N \left[ \partial^{\{\mu}, [\partial^{\nu\}}, V_{\mu\nu}^0] \right] \psi_N, \end{aligned} \quad (11)$$

where the first part of this Lagrangian is the interaction between the pion fields and the external isoscalar tensor field.  $x_\pi^0$  is the momentum fraction of the pion carried by quarks. Its value is less than 1 since some of the momentum of the pion is carried by gluons. In the preceding equations,  $a_{2,0}^v$ ,  $a_{2,0}^s$ ,  $b_{2,0}^v$ ,  $b_{2,0}^s$ ,  $c_{2,0}^v$  and  $c_{2,0}^s$  are the low energy constants which can be determined from the lattice data.

In our calculation, we also include the  $\Delta$  intermediate baryon, which is known to be crucial in the calculation of spin dependent quantities. The interaction between the  $\Delta$  and the external tensor field can be written as

$$\begin{aligned} \mathcal{L}_\Delta = & -ia_{2,0}^{v,d} T^\alpha \gamma^{\{\mu} \overleftrightarrow{D}^{\nu\}} T_\alpha V_{\mu\nu}^3 - \frac{ib_{2,0}^{v,d}}{M_N} T^\alpha \overleftrightarrow{D}^\nu T^\beta F_{\alpha\beta\nu}^3 + \frac{b_{2,0}^{v,t}}{2M_N} (\bar{T}^\alpha \gamma^\beta \overleftrightarrow{D}^\nu \psi + \bar{\psi} \gamma^\beta \overleftrightarrow{D}^\nu T^\alpha) F_{\alpha\beta\nu}^3 \\ & + \frac{c_{2,0}^{v,d}}{M_N} T^\alpha \left[ D^{\{\mu}, [D^{\nu\}}, V_{\mu\nu}^3] \right] T_\alpha - ia_{2,0}^{s,d} T^\alpha \gamma^{\{\mu} \overleftrightarrow{\partial}^{\nu\}} T_\alpha V_{\mu\nu}^0 - \frac{ib_{2,0}^{s,d}}{M_N} T^\alpha \overleftrightarrow{\partial}^\nu T^\beta F_{\alpha\beta\nu}^0 \\ & + \frac{c_{2,0}^{s,d}}{M_N} T^\alpha \left[ \partial^{\{\mu}, [\partial^{\nu\}}, V_{\mu\nu}^0] \right] T_\alpha, \end{aligned} \quad (12)$$

where  $F_{\alpha\beta\nu}^3 = [D_\alpha, V_{\beta\nu}^3] - [D_\beta, V_{\alpha\nu}^3]$  and  $F_{\alpha\beta\nu}^0 = [\partial_\alpha, V_{\beta\nu}^0] - [\partial_\beta, V_{\alpha\nu}^0]$ . The labels  $d$  and  $t$  in the low energy constants stand for decuplet and transition, respectively.  $T^\alpha$  are for decuplet fields which have three flavor indices (they are not shown explicitly, see for example, Ref. [50] for details), defined as

$$T_{111} = \Delta^{++}, \quad T_{112} = \Delta^+, \quad T_{122} = \Delta^0, \quad T_{222} = \Delta^-. \quad (13)$$

Within the framework of  $SU(6)$  symmetry, there are relationships between the octet and decuplet coefficients. For the isovector coefficients:

$$\begin{aligned} a_{2,0}^{v,\Delta^{++}} &= 3a_{2,0}^v, & a_{2,0}^{v,\Delta^+} &= a_{2,0}^v, & a_{2,0}^{v,\Delta^0} &= -a_{2,0}^v, & a_{2,0}^{v,\Delta^-} &= -3a_{2,0}^v, \\ b_{2,0}^{v,\Delta^{++}} &= \frac{9}{5}b_{2,0}^v, & b_{2,0}^{v,\Delta^+} &= \frac{3}{5}b_{2,0}^v, & b_{2,0}^{v,\Delta^0} &= -\frac{3}{5}b_{2,0}^v, & b_{2,0}^{v,\Delta^-} &= -\frac{9}{5}b_{2,0}^v, \\ c_{2,0}^{v,\Delta^{++}} &= 3c_{2,0}^v, & c_{2,0}^{v,\Delta^+} &= c_{2,0}^v, & c_{2,0}^{v,\Delta^0} &= -c_{2,0}^v, & c_{2,0}^{v,\Delta^-} &= -3c_{2,0}^v. \end{aligned} \quad (14)$$

For the isoscalar coefficients, we have:

$$\begin{aligned}
a_{2,0}^{s,\Delta^{++}} &= a_{2,0}^s, & a_{2,0}^{s,\Delta^+} &= a_{2,0}^s, & a_{2,0}^{s,\Delta^0} &= a_{2,0}^s, & a_{2,0}^{s,\Delta^-} &= a_{2,0}^s, \\
b_{2,0}^{s,\Delta^{++}} &= 3b_{2,0}^s, & b_{2,0}^{s,\Delta^+} &= 3b_{2,0}^s, & b_{2,0}^{s,\Delta^0} &= 3b_{2,0}^s, & b_{2,0}^{s,\Delta^-} &= 3b_{2,0}^s, \\
c_{2,0}^{s,\Delta^{++}} &= c_{2,0}^s, & c_{2,0}^{s,\Delta^+} &= c_{2,0}^s, & c_{2,0}^{s,\Delta^0} &= c_{2,0}^s, & c_{2,0}^{s,\Delta^-} &= c_{2,0}^s.
\end{aligned} \tag{15}$$

With the Lagrangian, we can calculate the form factors. In the case of the lowest moments, the electric form factor is related to the contribution from the time component of the vector current, while the magnetic form factor is related to the space component contribution. For the first form factors, similar as in the case of electric and magnetic form factors, one can also get three form factors  $\mathcal{A}_{2,0}$ ,  $\mathcal{B}_{2,0}$  and  $\mathcal{C}_{2,0}$  in the heavy baryon formalism, whose relationships to the tensor current are

$$J_{00}^q \equiv i\langle p' | \bar{q}\gamma_{\{0} \overleftrightarrow{D}_{0\}} | p \rangle = \frac{3\bar{p}_0}{2} \mathcal{A}_{2,0}^q(Q^2) + \frac{Q^2}{2M_N} \mathcal{C}_{2,0}^q(Q^2), \tag{16}$$

$$J_{33}^q \equiv i\langle p' | \bar{q}\gamma_{\{3} \overleftrightarrow{D}_{3\}} | p \rangle = \frac{\bar{p}_0}{2} \mathcal{A}_{2,0}^q(Q^2) + \frac{3Q^2}{2M_N} \mathcal{C}_{2,0}^q(Q^2), \tag{17}$$

$$J_{03}^q \equiv i\langle p' | \bar{q}\gamma_{\{0} \overleftrightarrow{D}_{3\}} | p \rangle = \frac{i\bar{p}_0}{2M_N} \mathcal{B}_{2,0}^q(Q^2) (\vec{\sigma} \times \vec{Q})_3. \tag{18}$$

Within the heavy baryon formalism these three form factors are related to the commonly used alternative form factors:

$$\mathcal{A}_{2,0}^q(Q^2) = A_{2,0}^q(Q^2) - \frac{Q^2}{8M_N(E + M_N)} A_{2,0}^q(Q^2) - \frac{Q^2}{4M_N^2} B_{2,0}^q(Q^2) \tag{19}$$

$$B_{2,0}^q(Q^2) = B_{2,0}^q(Q^2) + A_{2,0}^q(Q^2) - \frac{Q^2}{8M_N(E + M_N)} B_{2,0}^q(Q^2) \tag{20}$$

$$C_{2,0}^q(Q^2) = C_{2,0}^q(Q^2) + \frac{Q^2}{8M_N(E + M_N)} C_{2,0}^q(Q^2) \tag{21}$$

### III. FIRST MOMENTS OF GPDS

In this section, we will derive the formulas for the isovector and isoscalar form factors  $\mathcal{A}_{2,0}$ ,  $\mathcal{B}_{2,0}$  and  $\mathcal{C}_{2,0}$ . The one loop Feynman diagrams are shown in Fig. 1. The solid lines are for the nucleons and  $\Delta$ . The dashed lines are for the  $\pi$  meson and the dotted lines are for the external tensor current. Not all the diagrams have contribution to isoscalar or isovector form factors. From Eq. (11), one can see that there is no corresponding interaction between the pion and the isovector tensor field. This is because the  $\tau$  matrix is traceless. For the isoscalar form factors, the contributions of the  $\pi^+$  and  $\pi^-$  loops in diagram c cancel. As a result, diagram c gives no contribution to either the isoscalar or isovector form factors. In Fig. 1, graphs b, d and f are of order  $\mathcal{O}(m_\pi^2)$ , while e is of order  $\mathcal{O}(m_\pi^3)$ . The order of diagram a is dependent on the moments. Its order is of  $\mathcal{O}(m_\pi^3)$  for  $\mathcal{A}_{2,0}^q$ ,  $\mathcal{O}(m_\pi^2)$  for  $\mathcal{B}_{2,0}^q$  and  $\mathcal{O}(m_\pi)$  for  $\mathcal{C}_{2,0}^q$ . We study the isovector form factors first. For the isovector form factors, the diagram Fig. 1a and 1c have no contribution and diagram 1e only contributes to  $\mathcal{A}_{2,0}^q$ .

The contribution of Fig. 1b, including wave function renormalisation (Fig. 1f), is expressed as

$$\mathcal{A}_{2,0}^{v,b+f} = Z a_{2,0}^v - \frac{g_A^2 a_{2,0}^v}{64\pi^3 F_\pi^2} \int d^3k \frac{\vec{k}^2 u^2(\vec{k})}{\omega^3(\vec{k})} - \frac{5C^2 a_{2,0}^v}{72\pi^3 F_\pi^2} \int d^3k \frac{\vec{k}^2 u^2(\vec{k})}{\omega(\vec{k})(\omega(\vec{k}) + \delta)^2}, \tag{22}$$

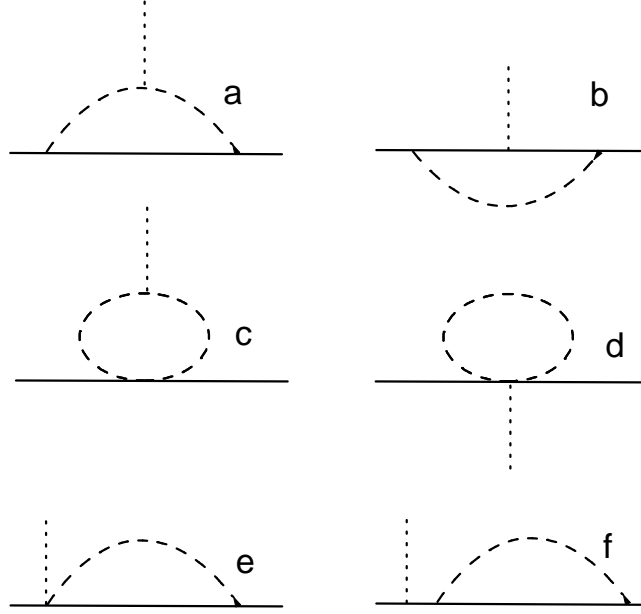


FIG. 1: One loop Feynman diagrams for the first moments of the GPDs. The solid, dashed and dotted lines are for nucleon(including  $\Delta$ ),  $\pi$  meson and external tensor current, respectively.

$$\begin{aligned} \mathcal{B}_{2,0}^{v,b+f} &= Zb_{2,0}^v + \frac{g_A^2 b_{2,0}^v}{192\pi^3 F_\pi^2} \int d^3k \frac{\vec{k}^2 u^2(\vec{k})}{\omega^3(\vec{k})} + \frac{5\mathcal{C}^2 b_{2,0}^v}{216\pi^3 F_\pi^2} \int d^3k \frac{\vec{k}^2 u^2(\vec{k})}{\omega(\vec{k})(\omega(\vec{k}) + \delta)^2} \\ &+ \frac{g_A \mathcal{C} b_{2,0}^v}{90\pi^3 F_\pi^2} \int d^3k \frac{\vec{k}^2 u^2(\vec{k})}{\omega(\vec{k})^2 (\omega(\vec{k}) + \delta)}, \end{aligned} \quad (23)$$

$$\mathcal{C}_{2,0}^{v,b+f} = Zc_{2,0}^v - \frac{g_A^2 c_{2,0}^v}{64\pi^3 F_\pi^2} \int d^3k \frac{\vec{k}^2 u^2(\vec{k})}{\omega^3(\vec{k})} - \frac{5\mathcal{C}^2 c_{2,0}^v}{72\pi^3 F_\pi^2} \int d^3k \frac{\vec{k}^2 u^2(\vec{k})}{\omega(\vec{k})(\omega(\vec{k}) + \delta)^2}, \quad (24)$$

where  $u(\vec{k})$  is the ultra-violet regulator and  $\omega(\vec{k}) = \sqrt{\vec{k}^2 + m_\pi^2}$ .  $\delta$  is the mass difference between nucleon and  $\Delta$ . In the above equations,  $\mathcal{C}$  is the nucleon- $\Delta$ - $\pi$  coupling constant [45]. The wave function renormalisation constant  $Z$  is expressed as

$$Z = 1 - \frac{3g_A^2}{64\pi^3 F_\pi^2} \int d^3k \frac{\vec{k}^2 u^2(\vec{k})}{\omega^3(\vec{k})} - \frac{\mathcal{C}^2}{24\pi^3 F_\pi^2} \int d^3k \frac{\vec{k}^2 u^2(\vec{k})}{\omega(\vec{k})(\omega(\vec{k}) + \delta)^2}. \quad (25)$$

The first integrals in the above formulas are from the intermediate nucleon contribution, while the second integrals are from the intermediate decuplet contribution. The third integral in Eq. (23) is from the  $N - \Delta$  transition. This transition contribution only exists for  $\mathcal{B}_{2,0}^v$ .

The contribution of Fig. 1d is obtained as

$$\mathcal{A}_{2,0}^{v,d} = -\frac{a_{2,0}^v}{16\pi^3 F_\pi^2} \int d^3k \frac{u^2(\vec{k})}{\omega(\vec{k})}, \quad (26)$$

$$\mathcal{B}_{2,0}^{v,d} = -\frac{b_{2,0}^v}{16\pi^3 F_\pi^2} \int d^3k \frac{u^2(\vec{k})}{\omega(\vec{k})}, \quad (27)$$

$$\mathcal{C}_{2,0}^{v,d} = -\frac{c_{2,0}^v}{16\pi^3 F_\pi^2} \int d^3k \frac{u^2(\vec{k})}{\omega(\vec{k})}, \quad (28)$$

Fig. 1e only contributes to the form factor  $\mathcal{A}_{2,0}$  expressed as

$$\mathcal{A}_{2,0}^{v,e} = \frac{g_A \Delta a_{2,0}^v}{48\pi^3 F_\pi^2 M_N} \int d^3k \frac{\vec{k}^2 u^2(\vec{k})}{\omega^2(\vec{k})}. \quad (29)$$

From the formulas one can see that in the heavy baryon formalism, the lowest order loop contribution to the isovector form factors are  $Q^2$  independent.

The total expression for the form factors can be written as

$$\mathcal{G}_{2,0}^v(Q^2, m_\pi^2) = Z(g_{2,0}^v + g_\pi^v m_\pi^2 + (g_t^v + g_{\pi,t}^v m_\pi^2)Q^2) + \sum_{i=a}^f \mathcal{G}_{2,0}^{v,i}, \quad (30)$$

where  $\mathcal{G}_{2,0}^v$  stands for  $\mathcal{A}_{2,0}^v$ ,  $\mathcal{B}_{2,0}^v$  and  $\mathcal{C}_{2,0}^v$ .  $g_{2,0}^v$ ,  $g_\pi^v$ ,  $g_t^v$  and  $g_{\pi,t}^v$  are the corresponding low energy constants which are determined by fitting the lattice data. In particular,  $g_{2,0}^v$  is identical to  $a_{2,0}^v$ ,  $b_{2,0}^v$  and  $c_{2,0}^v$ , correspondingly. The other terms in the above equations are from the tree level Lagrangian of high order. For example, for  $\mathcal{A}_{2,0}^v$ , the  $m_\pi^2$  dependent term can be obtained from the interaction  $\bar{\psi}_N \left\{ [u^\dagger V_{\mu\nu}^3 \tau^3 u + u V_{\mu\nu}^3 \tau^3 u^\dagger] \langle \chi_+ \rangle \gamma^{\{\mu} \overleftrightarrow{D}^{\nu\}} \right\} \psi_N$ , where  $\chi_+ = u^\dagger \chi u^\dagger + u \chi^\dagger u$  and  $\chi = 2B\mathcal{M}$ .  $B$  is the chiral condensate and  $\mathcal{M}$  is the quark mass matrix.  $\langle \dots \rangle$  denotes the trace in flavor space. The  $Q^2$  dependent term comes from the interaction  $\bar{\psi}_N \left\{ [D^\alpha, [D_\alpha, u^\dagger V_{\mu\nu}^3 \tau^3 u + u V_{\mu\nu}^3 \tau^3 u^\dagger]] \gamma^{\{\mu} \overleftrightarrow{D}^{\nu\}} \right\} \psi_N$ .

Since in the heavy baryon formalism, the loop contribution is  $Q^2$  independent, the  $Q^2$  dependence appears only in the analytic part. One can also fit the data versus  $Q^2$  at fixed pion mass. In that case Eq. (30) becomes:

$$\mathcal{G}_{2,0}^v(Q^2)|_{fixed\ m_\pi^2} = Z(h_1^v + h_2^v Q^2) + \sum_{i=a}^f \mathcal{G}_{2,0}^{v,i}, \quad (31)$$

where  $h_1^v$  and  $h_2^v$  are fitted independently for each pion mass.

For the isoscalar form factors, Fig. 1a, Fig. 1b and Fig. 1f contribute, while fig. 1c and 1d give no contribution. The reason is that in Fig. 1c and 1d, the  $\pi^+$  and  $\pi^-$  loops cancel each other exactly. The contributions from 1b and 1f are

$$\mathcal{A}_{2,0}^s = Z a_{2,0}^s + \frac{3g_A^2 a_{2,0}^s}{64\pi^3 F_\pi^2} \int d^3k \frac{\vec{k}^2 u^2(\vec{k})}{\omega^3(\vec{k})} + \frac{\mathcal{C}^2 a_{2,0}^s}{8\pi^3 F_\pi^2} \int d^3k \frac{\vec{k}^2 u^2(\vec{k})}{\omega(\vec{k})(\omega(\vec{k}) + \delta)^2}, \quad (32)$$

$$\mathcal{B}_{2,0}^s = Z b_{2,0}^s - \frac{3g_A^2 b_{2,0}^s}{192\pi^3 F_\pi^2} \int d^3k \frac{\vec{k}^2 u^2(\vec{k})}{\omega^3(\vec{k})} - \frac{5\mathcal{C}^2 b_{2,0}^s}{72\pi^3 F_\pi^2} \int d^3k \frac{\vec{k}^2 u^2(\vec{k})}{\omega(\vec{k})(\omega(\vec{k}) + \delta)^2}, \quad (33)$$

$$\mathcal{C}_{2,0}^s = Z c_{2,0}^s + \frac{3g_A^2 c_{2,0}^s}{64\pi^3 F_\pi^2} \int d^3k \frac{\vec{k}^2 u^2(\vec{k})}{\omega^3(\vec{k})} + \frac{\mathcal{C}^2 c_{2,0}^s}{8\pi^3 F_\pi^2} \int d^3k \frac{\vec{k}^2 u^2(\vec{k})}{\omega(\vec{k})(\omega(\vec{k}) + \delta)^2}. \quad (34)$$

Again, the first integrals of the above three formulas are from the nucleon and the second integrals are from the  $\Delta$  intermediate state.

To evaluate Fig. 1a, we need to calculate the contribution of three components of the tensor current defined in Eqs. (16)-(18). The expression for these components are

$$J_{00}^s = -\frac{3g_A^2 x_\pi^0}{128\pi^3 F_\pi^2} \int d^3k \frac{u(\vec{k})u(\vec{k}-\vec{q})[\vec{k} \cdot (\vec{k}-\vec{q})]^2}{\omega^2(\vec{k})\omega^2(\vec{k}-\vec{q})} - \frac{\mathcal{C}^2 x_\pi^0}{48\pi^3 F_\pi^2} \int d^3k u(\vec{k})u(\vec{k}-\vec{q})[\vec{k} \cdot (\vec{k}-\vec{q})]^2 f(\omega), \quad (35)$$

$$\begin{aligned} J_{33}^s &= -\frac{3g_A^2 x_\pi^0}{128\pi^3 F_\pi^2} \int d^3k \frac{u(\vec{k})u(\vec{k}-\vec{q})[4k_z(k_z - q_z) - \vec{k} \cdot (\vec{k}-\vec{q})]\vec{k} \cdot (\vec{k}-\vec{q})}{\omega^2(\vec{k})\omega^2(\vec{k}-\vec{q})} \\ &\quad - \frac{\mathcal{C}^2 x_\pi^0}{48\pi^3 F_\pi^2} \int d^3k u(\vec{k})u(\vec{k}-\vec{q})[4k_z(k_z - q_z) - \vec{k} \cdot (\vec{k}-\vec{q})]\vec{k} \cdot (\vec{k}-\vec{q}) f(\omega), \end{aligned} \quad (36)$$

$$\begin{aligned}
J_{03}^s = & \frac{i3g_A^2 x_\pi^0}{32\pi^3 F_\pi^2} \int d^3k \frac{u(\vec{k})u(\vec{k}-\vec{q})k_z^2(\vec{\sigma} \times \vec{q})_z}{\omega(\vec{k})\omega(\vec{k}-\vec{q})[\omega(\vec{k}) + \omega(\vec{k}-\vec{q})]} \\
& - \frac{i\mathcal{C}^2 x_\pi^0}{24\pi^3 F_\pi^2} \int d^3k \frac{u(\vec{k})u(\vec{k}-\vec{q})k_z^2(\vec{\sigma} \times \vec{q})_z}{[\omega(\vec{k}) + \delta][\omega(\vec{k}-\vec{q}) + \delta][\omega(\vec{k}) + \omega(\vec{k}-\vec{q})]},
\end{aligned} \tag{37}$$

where  $f(\omega)$  is expressed as

$$f(\omega) = \frac{\omega(\vec{k}) + \omega(\vec{k}-\vec{q}) + \delta}{\omega(\vec{k})[\omega(\vec{k}) + \delta]\omega(\vec{k}-\vec{q})[\omega(\vec{k}-\vec{q}) + \delta][\omega(\vec{k}) + \omega(\vec{k}-\vec{q})]}. \tag{38}$$

Both the intermediate nucleon and  $\Delta$  states are included. One can see that this diagram gives the  $Q^2$  dependence of the form factors. The total isoscalar form factors  $\mathcal{A}_{2,0}^s$ ,  $\mathcal{B}_{2,0}^s$  and  $\mathcal{C}_{2,0}^s$  can be written in the same way as Eq. (30). The corresponding low energy constants can also be determined by the lattice data.

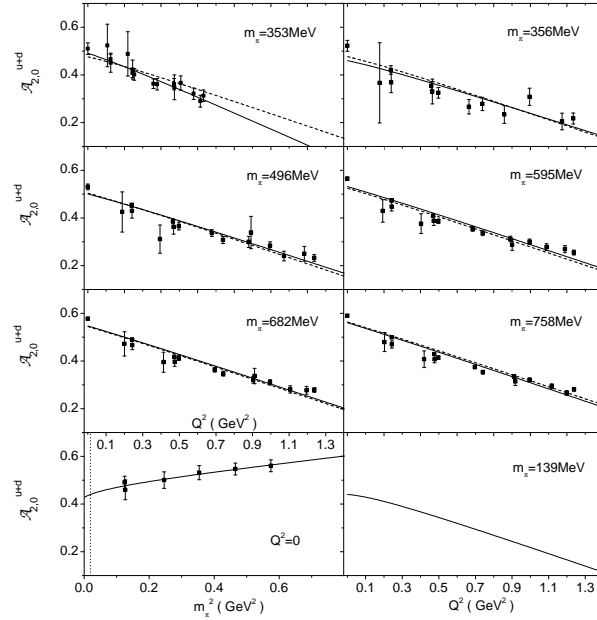


FIG. 2: The form factor  $\mathcal{A}_{2,0}^{u+d}$  versus  $Q^2$  at each pion mass and versus pion mass at  $Q^2 = 0$ . The dashed and solid lines correspond to the global and separate fit to the lattice data, respectively.

#### IV. NUMERICAL RESULTS

In the numerical calculations, the parameters are chosen to be  $D = 0.76$  and  $F = 0.50$  ( $g_A = D + F = 1.26$ ). The coupling constant  $\mathcal{C}$  is chosen to be  $-2D$ , as estimated by  $SU(6)$  relations — which gives a similar value to that obtained from the hadronic decay width of the  $\Delta$ . Here the finite-range regulator is chosen to take the dipole form

$$u(\vec{k}) = \frac{1}{(1 + \vec{k}^2/\Lambda^2)^2}, \tag{39}$$

with  $\Lambda = 0.8$  GeV. The regulator has been applied in our previous work on nucleon mass, magnetic moments, form factors, charge radii, etc. The other two parameters in the Lagrangian  $x_\pi^0$  and  $\Delta a_{2,0}^v$  are chosen to be 0.7 [51] and 0.21 [35], respectively.

All the lattice data had been transformed to a scale of  $\mu^2 = 4$  GeV<sup>2</sup>. We first study the isoscalar form factors. The form factor  $\mathcal{A}_{2,0}^{u+d}$  is shown in Fig. 2. The lattice data are from Ref. [29]. The solid lines correspond to fitting

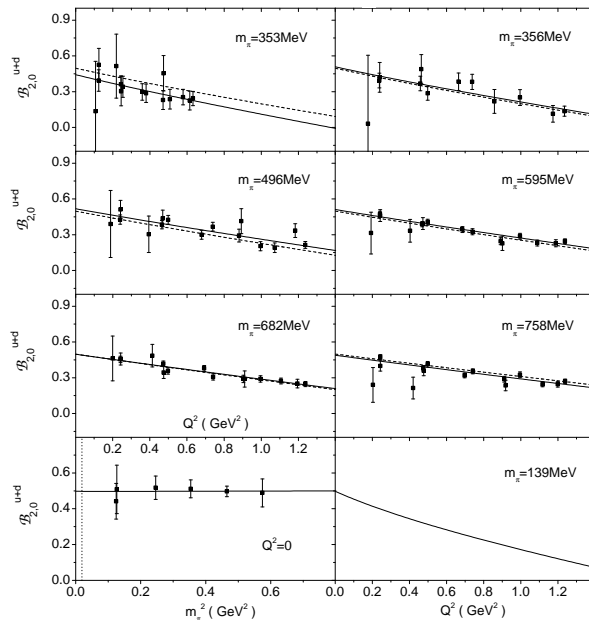


FIG. 3: The form factor  $\mathcal{B}_{2,0}^{u+d}$  versus  $Q^2$  at each pion mass and versus pion mass at  $Q^2 = 0$ . The dashed and solid lines correspond to the global and separate fits to the lattice data, respectively.

the lattice data with Eq. (31) at each pion mass separately. The dashed lines correspond to fitting the lattice data with Eq. (30) for all the pion masses. We can see from the figure that the difference between the solid and dashed lines is relatively small. Both of them can extrapolate the lattice data very well. At each pion mass, the lattice data shows a dependence on  $Q^2$  which is almost linear. In fact, the result of the Fig. 1 is  $Q^2$  independent except for Fig.1a, which gives a little curvature to the line. It is interesting that the momentum dependence of the first form factor is not like the electromagnetic form factor which has a dipole behavior. For the  $m_\pi$  dependence, it is not like the electromagnetic moment either. For example, For the magnetic moment, Fig. 1a gives the leading order of  $\mathcal{O}(m_\pi)$  contribution. For  $\mathcal{A}_{2,0}^{u+d}$ , the leading order is of  $\mathcal{O}(m_\pi^2)$ . This is because in this case, Fig. 1a are of  $\mathcal{O}(m_\pi^3)$ . Fig. 1b and Fig. 1f are of  $\mathcal{O}(m_\pi^2)$  which is the same for the magnetic form factor. Therefore, the magnetic form factor has a large curvature at small pion mass. At  $Q^2 = 0$ ,  $\mathcal{A}_{2,0}^{u+d}$  increases with increasing pion mass.

The form factor  $\mathcal{B}_{2,0}^{u+d}$  is shown in Fig. 3. The solid and dashed lines have the same meaning as in Fig. 2. Again, the lattice data can be described very well. Similarly to  $\mathcal{A}_{2,0}^{u+d}$ ,  $\mathcal{B}_{2,0}^{u+d}$  has little curvature with increasing  $Q^2$ . The form factor is not sensitive to the pion mass. For this form factor, all the diagrams in Fig. 1 are of  $\mathcal{O}(m_\pi^2)$  including Fig. 1a. At the physical pion mass, the value of  $\mathcal{B}_{2,0}^{u+d}$  at  $Q^2 = 0$  is  $0.497 \pm 0.089$ .

From Ji's sum rule [52], the relationship between the moments and the quark contribution to the total nucleon spin is

$$J_{u+d} = \frac{1}{2}[A_{2,0}^s(Q^2 = 0) + B_{2,0}^s(Q^2 = 0)] = \frac{1}{2}\mathcal{B}_{2,0}^s(Q^2 = 0). \quad (40)$$

With the extrapolated value of  $\mathcal{B}_{2,0}^s(Q^2 = 0)$  at the physical pion mass, we find  $J_{u+d} = 0.249 \pm 0.045$ . Since the total spin of the nucleon is 1/2, it is interesting that only 50% of the nucleon spin is carried by quarks. This is consistent with studies of the evolution of the total quark angular momentum from a scale typical of a valence-dominated quark model [9].

In Fig. 4 we show the form factor  $\mathcal{C}_{2,0}^{u+d}$ . Once again the  $Q^2$  dependence shows little curvature. However, this time, the  $m_\pi$  dependence has a visible curvature at the physical pion mass and  $Q^2 = 0$ . This is because, unlike  $\mathcal{A}_{2,0}^{u+d}$  and  $\mathcal{B}_{2,0}^{u+d}$ , Fig. 1a has a leading nonanalytic term of order  $\mathcal{O}(m_\pi)$  for  $\mathcal{C}_{2,0}^{u+d}$ . The absolute value of  $\mathcal{C}_{2,0}^{u+d}$  decreases with increasing pion mass at  $Q^2 = 0$ .



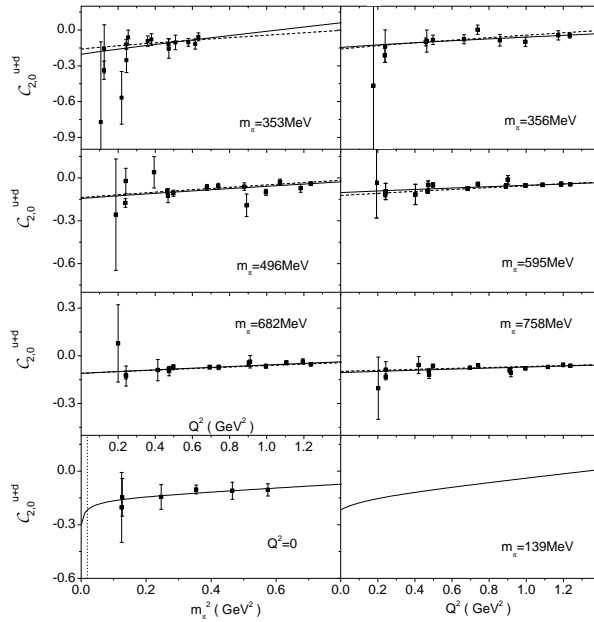


FIG. 4: The form factor  $C_{2,0}^{u+d}$  versus  $Q^2$  at each pion mass and versus pion mass at  $Q^2 = 0$ . The dashed and solid lines correspond to the global and separate fits to the lattice data, respectively.

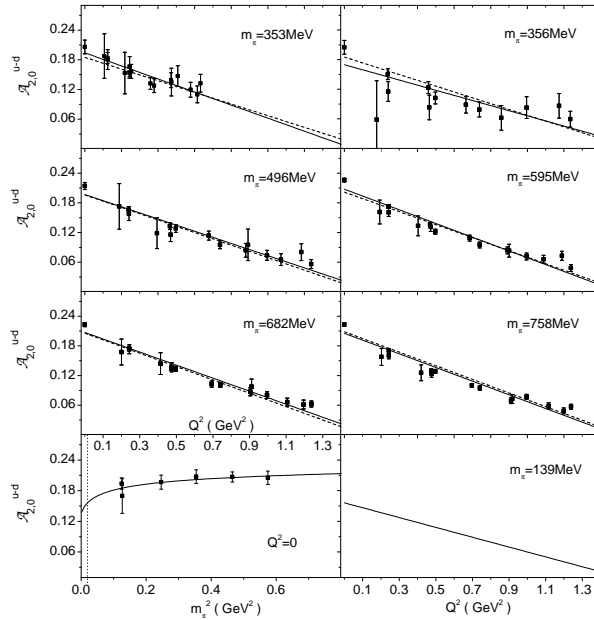


FIG. 5: The form factor  $A_{2,0}^{u-d}$  versus  $Q^2$  at each pion mass and versus pion mass at  $Q^2 = 0$ . The dashed and solid lines correspond to the global and separate fits to the lattice data, respectively.

Having discussed the isoscalar moments which describe the total contribution of the  $u$  and  $d$  quark, we now turn to the isovector part. The isovector moments describe the difference of the  $u$  and  $d$  quark contributions. In this case, diagram a and c in Fig. 1 have no contribution and, as a result, the isovector form factors of the loop are  $Q^2$  independent. The form factor  $A_{2,0}^{u-d}$  is shown in Fig. 5. Just as for the isoscalar form factors, the diagrams of Fig. 1b, 1d and 1f are of  $\mathcal{O}(m_\pi^2)$ . Because Fig. 1e is of  $\mathcal{O}(m_\pi^3)$ , the result is not sensitive to the choice of  $\Delta a_{2,0}^v$ . For example, at  $Q^2 = 0$ , the values of  $A_{2,0}^{u-d}$  are 0.156 and 0.153 for  $\Delta a_{2,0}^v = 0.21$  (phenomenological value) and 0.144 (fit value), respectively [35, 36]. For the  $Q^2$  dependence, from the figure one can see that the lines are well described by a linear dependence on  $Q^2$ , which comes from the choice of tree level contribution.

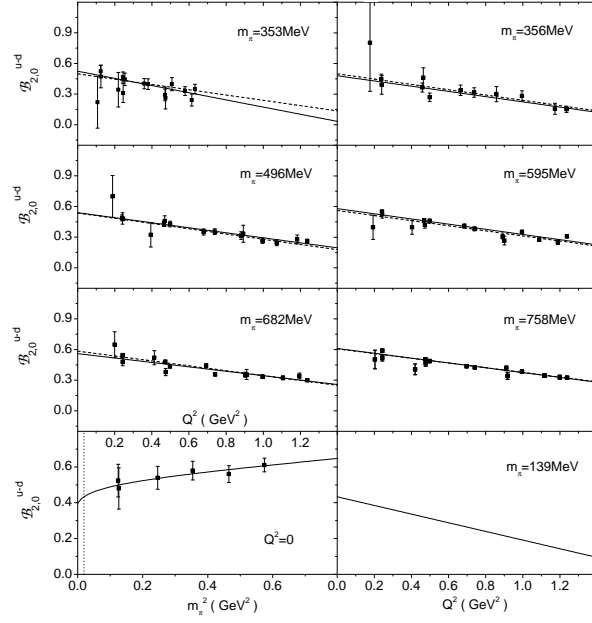


FIG. 6: The form factor  $\mathcal{B}_{2,0}^{u-d}$  versus  $Q^2$  at each pion mass and versus pion mass at  $Q^2 = 0$ . The dashed and solid lines correspond to the global and separate fits to the lattice data, respectively.

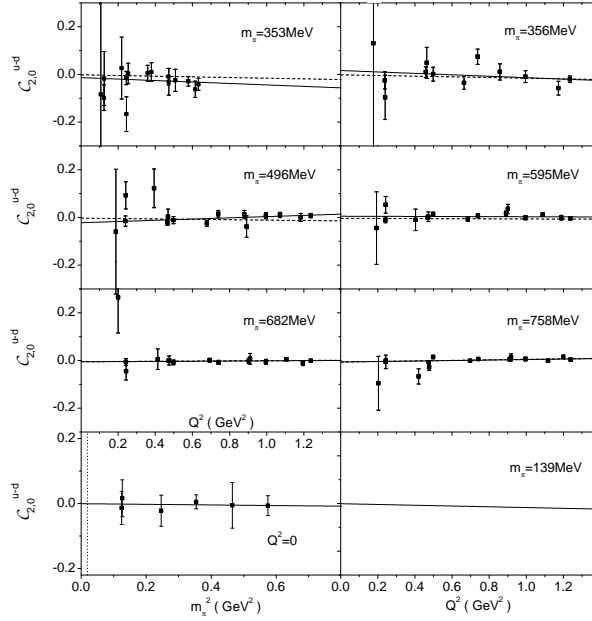


FIG. 7: The form factor  $\mathcal{C}_{2,0}^{u-d}$  versus  $Q^2$  at each pion mass and versus pion mass at  $Q^2 = 0$ . The dashed and solid lines correspond to the global and separate fits to the lattice data, respectively.

In Fig. 6 we show the isovector form factor  $\mathcal{B}_{2,0}^{u-d}$ . At  $Q^2 = 0$ , it increases with increasing  $m_\pi^2$ . At the physical pion mass its value is about  $0.433 \pm 0.071$ .  $\mathcal{B}_{2,0}^{u-d}$  is close to  $\mathcal{B}_{2,0}^{u+d}$ , which means that the  $u$  quark is dominant for the proton spin while the  $d$  quark gives little contribution. The form factor  $\mathcal{C}_{2,0}^{u-d}$  is shown in Fig. 7. The value of  $\mathcal{C}_{2,0}^{u-d}$  is around zero and not sensitive to either  $Q^2$  or  $m_\pi^2$ .

TABLE I: Low energy constants and moments at physical pion mass. The results in the table are for the linear fit where the momentum dependence of the tree level term is up to  $Q^2$ . For the dipole fit, the first moments at  $Q^2 = 0$  are about 10% – 20% larger. The results of LHPC are also listed in the last column.

	$g_{2,0}$	$g_\pi(\text{GeV}^{-2})$	$g_t(\text{GeV}^{-2})$	$g_{\pi,t}(\text{GeV}^{-4})$	$\mathcal{G}_{2,0}(0)$	$\mathcal{G}_{2,0}^{\text{LHPC}}(0)[29]$
$\mathcal{A}_{2,0}^{u+d}$	0.489	0.152	-0.266	0.019	$0.440 \pm 0.033$	$0.520 \pm 0.024$
$\mathcal{B}_{2,0}^{u+d}$	0.496	0.005	-0.339	0.268	$0.497 \pm 0.089$	$0.425 \pm 0.086$
$\mathcal{C}_{2,0}^{u+d}$	-0.152	0.102	0.119	-0.159	$-0.217 \pm 0.103$	$-0.267 \pm 0.062$
$\mathcal{A}_{2,0}^{u-d}$	0.207	0.010	-0.139	-0.009	$0.156 \pm 0.020$	$0.157 \pm 0.010$
$\mathcal{B}_{2,0}^{u-d}$	0.526	0.158	-0.298	0.111	$0.433 \pm 0.071$	$0.430 \pm 0.063$
$\mathcal{C}_{2,0}^{u-d}$	-0.001	-0.009	-0.025	0.062	$-0.001 \pm 0.050$	$-0.017 \pm 0.041$

The values of  $\mathcal{A}_{2,0}$ ,  $\mathcal{B}_{2,0}$  and  $\mathcal{C}_{2,0}$  at the physical pion mass and  $Q^2 = 0$  are shown in Table I. Using Eqs. (19)-(21), one can extract the form factors  $A_{2,0}$ ,  $B_{2,0}$  and  $C_{2,0}$ . In particular, at  $Q^2 = 0$ ,  $\mathcal{A}_{2,0} = A_{2,0}$ ,  $\mathcal{B}_{2,0} = A_{2,0} + B_{2,0}$  and  $\mathcal{C}_{2,0} = C_{2,0}$ . Compared with those in Ref. [29] extrapolated with the formulas in Ref. [35], our numerical results are close to their results which used dimensional regularization. With the values for the isoscalar and isovector moments in the Table, one can easily find the  $u$  and  $d$  quark moments. For example, for the moment  $\mathcal{A}_{2,0}$ , the contribution from the  $u$  quark is about as twice large as that from the  $d$  quark. This is because in the proton, there are two  $u$  quarks and one  $d$  quark. The values of the quark spin are  $J_u = 0.233 \pm 0.04$  and  $J_d = 0.016 \pm 0.04$ . The  $u$  quark dominance for the moment  $\mathcal{B}_{2,0}$  can be understood from the naive quark model for proton, where the  $u$  quark spin is as four times large as the  $d$  quark spin. For  $\mathcal{C}_{2,0}$ , it seems that the  $u$  and  $d$  quarks yield almost the same contribution.

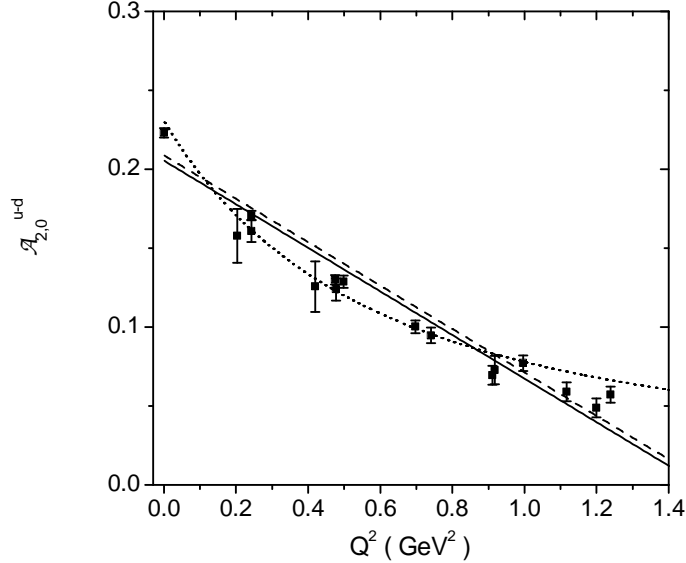


FIG. 8: The form factor  $\mathcal{A}_{2,0}^{u-d}$  versus  $Q^2$  at  $m_\pi = 758$  MeV. The solid and dashed lines are for the linear fit as in Fig. 5. The dotted line is for the dipole fit.

We should mention that our extrapolation results depend on the choice of the tree-level contribution. In the previous fit, the order of the momentum dependence of the tree-level contribution is up to  $Q^2$ . This is supposed to be valid at low momentum transfer. We know that for the electromagnetic form factors, the momentum dependence has a dipole behavior with mass parameter around  $0.71 \text{ GeV}^2$ . In the case of the axial form factor, which is perhaps more relevant for the spin distribution, the phenomenological form factor is a  $1 \text{ GeV}$  dipole. Since the actual lattice data extends over such a broad range of  $Q^2$ , a pure linear dependence on  $Q^2$  is difficult to justify. Therefore, we have carried out another fit with a modified dipole form. The  $Q^2$  dependence of the first moments, i.e. Eq. (31), is now changed to the following expression:

$$\mathcal{G}_{2,0}^v(Q^2)|_{\text{fixed } m_\pi} = \frac{Z(h_1^v + h_2^v Q^2)}{(1 + Q^2/\Lambda^2)^2} + \sum_{i=a}^f \mathcal{G}_{2,0}^{v,i} \quad (41)$$

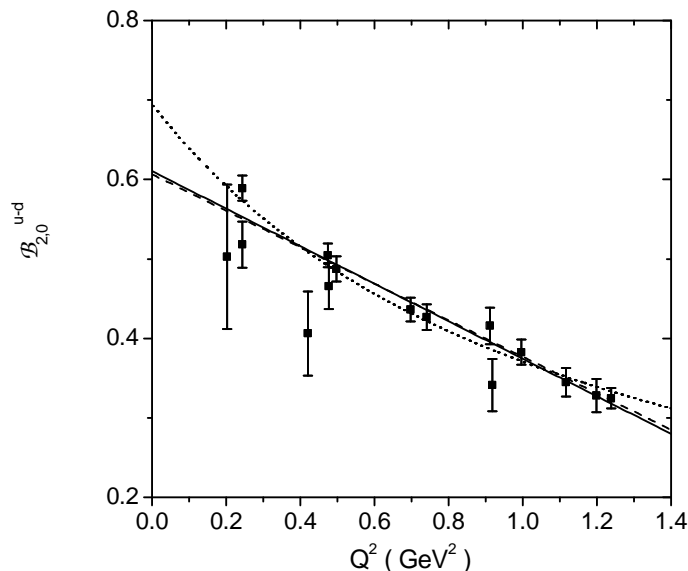


FIG. 9: The form factor  $\mathcal{B}_{2,0}^{u-d}$  versus  $Q^2$  at  $m_\pi = 758$  MeV. The solid and dashed lines are for the linear fit as in Fig. 6. The dotted line is for the dipole fit.

where  $\Lambda$  is chosen to be 1 GeV. While a pure dipole form would be preferred phenomenologically, we note that the data from Ref. [29] tends to give much harder form factors for the axial channel than those found in nature. The reason for this is not understood but our modified form allows room to fit the lattice data while still including some physically reasonable  $Q^2$  dependence.

We show the momentum dependence of  $\mathcal{A}_{2,0}^{u-d}$  and  $\mathcal{B}_{2,0}^{u-d}$  at  $m_\pi = 758$  MeV in Fig. 8 and Fig. 9. As a comparison, the solid and dashed lines with the previous linear fit are also shown. The dotted lines correspond to the fit with the modified dipole form at tree level. The lattice data can be reasonably described with both forms. For  $\mathcal{B}_{2,0}^{u-d}$ , compared with the linear fit, the dipole fit gives a larger value at  $Q^2 = 0$ . The situation is similar for the other pion masses. The curve of mass dependence of  $\mathcal{B}_{2,0}^{u-d}$  in Fig. 6 is shifted up in the dipole fit. As a result, the moment at the physical mass is increased from 0.433 to 0.53. For  $\mathcal{A}_{2,0}^{u-d}$ , the difference between two fits is not as large as for  $\mathcal{B}_{2,0}^{u-d}$ . This is because the lattice data for  $\mathcal{A}_{2,0}^{u-d}$  at  $Q^2 = 0$  impose a strong constraint in that case. At the physical pion mass, its value changes from 0.156 to 0.17.

The dipole fit makes the absolute value of all the first moments larger at  $Q^2 = 0$ . For  $\mathcal{A}_{2,0}$ , the difference is about 10% with the help of the lattice data at zero momentum. For  $\mathcal{B}_{2,0}$  and  $\mathcal{C}_{2,0}^{u+d}$ , the difference is about 20%. The value of  $\mathcal{C}_{2,0}^{u+d}$  is still around zero. The difference between these two separate fitting procedures provides some indication of the systematic error in extracting this important physical information from the lattice data.

## V. SUMMARY

Chiral perturbation theory with finite-range-regularization has been applied to the problem of extrapolating lattice QCD data for GPD moments to the physical pion mass and zero momentum transfer. For the isovector form factors, the one loop contribution is of  $\mathcal{O}(m_\pi^2)$ . For the isoscalar form factors,  $\mathcal{A}_{2,0}^{u+d}$  and  $\mathcal{B}_{2,0}^{u+d}$ , the leading order is of  $\mathcal{O}(m_\pi^2)$ , while for  $\mathcal{C}_{2,0}^{u+d}$ , the leading order is of  $\mathcal{O}(m_\pi)$ . The lattice data were fitted both globally and separately at each pion mass. At  $Q^2 = 0$ , the  $m_\pi$  dependence of the first moments (except  $\mathcal{C}_{2,0}^{u+d}$ ) does not show a big degree of curvature at small pion mass, which is quite different from the zero-th moments (electromagnetic form factors). Overall the level of agreement between the extrapolated results obtained using dimensional regularization and FRR is satisfactory.

The  $Q^2$  dependence, especially of  $\mathcal{B}_{2,0}$ , is mainly determined by the tree level  $Q^2$  behavior. In our first calculation, we retained only the tree level terms up to  $Q^2$ , that is a linear dependence. On the other hand, the data has been determined over a wide range of  $Q^2$ , up to 1.2 GeV<sup>2</sup>. Phenomenologically one knows that the physical form factors exhibit a considerable variation with  $Q^2$  over such a range – usually described by a dipole form. In order to test the sensitivity to this problem, we have re-done the fits to the lattice data using a modified dipole form. In this case the first moments at  $Q^2 = 0$  are about 10% – 20% larger than those in the linear fit. We regard this as a measure of one

of the main systematic errors associated with extracting information about the quark angular momentum.

In our calculation, the  $\Delta$  contributions have been included explicitly, because of its potential importance for spin dependent quantities. For the nucleon spin, the inclusion of the  $\Delta$  changes the result by 10% [7]. However, for the extrapolation of the first moments of GPDs, if the  $\Delta$  is not included the low energy constants are different. Since they are adjusted by fitting the lattice data, the extrapolated moments at the physical pion mass change by less than about 5% when the  $\Delta$  is included.

Using the extrapolated moment  $\mathcal{B}_{2,0}$ , we can extract information concerning the quark contribution to the nucleon spin. Our results are consistent with the current JLab and HERMES experiments [53, 54]. On the other hand, the experimental errors there are quite large at the present time. The comparison with model predictions, such as those of Refs. [7, 9], is also quite satisfactory, especially given the systematic errors associated with the  $Q^2$  dependence of  $\mathcal{B}_{2,0}$  (discussed above) and the dependence of the proton axial charge on lattice volume. As for the other two moments, the  $u$  quark contribution is twice as large as that for the  $d$  quark in  $\mathcal{A}_{2,0}$ , while they give similar contributions to  $\mathcal{C}_{2,0}$ . In comparing with data, it is important to note the possible sensitivity of isoscalar quantities to disconnected graphs which were not included in the LHPC simulation. In the next few years we can look forward not only to more accurate data on GPDs but lattice QCD data on larger volumes and at lower quark masses and, ideally, including disconnected terms. All of this offers enormous promise towards unravelling the proton spin problem.

### Acknowledgements

This work was supported by DOE contract No. DE-AC06-05OR23177 and by the Australian Research Council grant of an Australian Laureate Fellowship to AWT.

- 
- [1] A. W. Thomas and W. Weise, “The Structure of the Nucleon”, *Berlin, Germany: Wiley-VCH (2001) 389 p*
  - [2] X. Ji, *J. Phys. G* **24** (1998) 1181.
  - [3] A. V. Belitsky and A. V. Radyushkin, *Phys. Rept.* **418** (2005) 1.
  - [4] X. D. Ji, J. Tang and P. Hoodbhoy, *Phys. Rev. Lett.* **76**, 740 (1996) [arXiv:hep-ph/9510304].
  - [5] J. Ashman *et al.* [European Muon Collaboration], *Nucl. Phys. B* **328**, 1 (1989).
  - [6] S. D. Bass, *Rev. Mod. Phys.* **77**, 1257 (2005) [arXiv:hep-ph/0411005].
  - [7] F. Myhrer and A. W. Thomas, *Phys. Lett. B* **663**, 302 (2008) [arXiv:0709.4067 [hep-ph]].
  - [8] A. W. Schreiber and A. W. Thomas, *Phys. Lett. B* **215**, 141 (1988).
  - [9] A. W. Thomas, *Phys. Rev. Lett.* **101**, 102003 (2008) [arXiv:0803.2775 [hep-ph]].
  - [10] M. Guidal, M.V. Polyakov, A.V. Radyushkin, and M. Vanderhaeghen, *Phys. Rev. D* **72** (2005) 054013.
  - [11] X. Ji, W. Melnitchouk, and X. Song, *Phys. Rev. D* **56** (1997) 5511.
  - [12] B. Pasquini and S. Boffi, *Nucl. Phys. A* **782** (2007) 86
  - [13] S. Boffi, B. Pasquini, and M. Traini, *Nucl. Phys. B* **649** (2003) 243.
  - [14] S. Scopetta and V. Vento, *Phys. Rev. D* **69** (2004) 094004.
  - [15] H. Mineo, S.N. Yang, C.Y. Cheung and W. Bentz, *Phys. Rev. C* **72** (2005) 025202.
  - [16] H.-M. Choi, C.-R. Ji, and L.S. Kisslinger, *Phys. Rev. D* **64** (2001) 093006.
  - [17] H.-M. Choi, C.-R. Ji, and L.S. Kisslinger, *Phys. Rev. D* **66** (2002) 053011.
  - [18] K. Goeke, V. Guzey and M. Siddidov, *Eur. Phys. J. C* **56** (2008) 203.
  - [19] B.C. Tiburzi and G.A. Miller, *Phys. Rev. D* **65** (2002) 074009.
  - [20] L. Theussl, S. Noguera, and V. Vento, *Eur. Phys. J. A* **20** (2004) 483.
  - [21] P.R.B. Saull (ZEUS Coll.), hep-ex/0003030.
  - [22] C. Adloff *et al.* (HI Coll.), *Phys. Lett. B* **517** (2001) 47.
  - [23] N. d’Hose *et al.* (COMPASS Coll.), *AIP Conf. Proc.* **1160** (2009) 49.
  - [24] A. Airapetian *et al.* (HERMES Coll.), *Phys. Rev. Lett.* **87** (2001) 182001.
  - [25] A. Airapetian *et al.* (HERMES Coll.), arXiv:0911.0095.
  - [26] S. Chen *et al.* (CLAS Coll.), *Phys. Rev. Lett.* **87** (2006) 182002.
  - [27] A. Biselli *et al.* (CLAS Coll.), *AIP Conf. Proc.* **1149** (2009) 611.
  - [28] H. Egiyan *et al.* (CLAS Coll.), *AIP Conf. Proc.* **1149** (2009) 607.
  - [29] LHPC Collaborations (Ph. Haegler *et al.*), *Phys. Rev. D* **77** (2008) 094502
  - [30] QCDSF Collaboration (M. Gockeler *et al.*), *Phys. Rev. Lett.* **92** (2004) 042002
  - [31] QCDSF Collaboration and UKQCD Collaboration (D. Brommel *et al.*), *Phys. Rev. Lett.* **101** (2008) 122001.
  - [32] A. W. Thomas, *Nucl. Phys. Proc. Suppl.* **119**, 50 (2003) [arXiv:hep-lat/0208023].
  - [33] R. D. Young, D. B. Leinweber and A. W. Thomas, *Prog. Part. Nucl. Phys.* **50**, 399 (2003) [arXiv:hep-lat/0212031].
  - [34] D. B. Leinweber, A. W. Thomas and R. D. Young, *Nucl. Phys. A* **755**, 59 (2005) [arXiv:hep-lat/0501028].
  - [35] M. Dorati, T. A. Gail and T. R. Hemmert, *Nucl. Phys. A* **798** (2008) 96

- [36] M. Dorati, T. A. Gail and T. R. Hemmert, PoS LAT2007 (2007) 071.
- [37] M. Diehl, A. Manashov and A. Schafer, Eur. Phys. J. A **31** (2007) 335.
- [38] D. B. Leinweber, D. H. Lu and A. W. Thomas, Phys. Rev. D **60**, 034014 (1999) [arXiv:hep-lat/9810005].
- [39] D. B. Leinweber, A. W. Thomas, K. Tsushima and S. V. Wright, Phys. Rev. D **61** (2000) 074502.
- [40] D. B. Leinweber, A. W. Thomas and R. D. Young, Phys. Rev. Lett. **92**, 242002 (2004) [arXiv:hep-lat/0302020].
- [41] C. R. Allton, W. Armour, D. B. Leinweber, A. W. Thomas and R. D. Young, Phys. Lett. B **628** (2005) 125.
- [42] W. Armour *et al.*, J. Phys. G **32** (2006) 971.
- [43] R. D. Young, D. B. Leinweber and A. W. Thomas, Phys. Rev. D **71** (2005) 014001
- [44] P. Wang, A. W. Thomas, D. B. Leinweber and R. D. Young, Phys. Rev. D **75** (2007) 073012.
- [45] P. Wang, A. W. Thomas, D. B. Leinweber and R. D. Young, Phys. Rev. D **79** (2009) 094001.
- [46] P. Wang, A. W. Thomas, D. B. Leinweber and R. D. Young, Phys. Rev. C **79** (2009) 065202.
- [47] D. B. Leinweber *et al.*, Phys. Rev. Lett. **94**, 212001 (2005) [arXiv:hep-lat/0406002].
- [48] D. B. Leinweber *et al.*, Phys. Rev. Lett. **97**, 022001 (2006) [arXiv:hep-lat/0601025].
- [49] D. B. Leinweber *et al.*, Eur. Phys. J. A **24S2**, 79 (2005) [arXiv:hep-lat/0502004].
- [50] J. N. Labrenz and S. R. Sharpe, Phys. Rev. D **54** (1996) 4595.
- [51] A. V. Belitsky and X. Ji, Phys. Lett. B **538** (2002) 289.
- [52] X. Ji, Phys. Rev. Lett. **78** (1997) 610.
- [53] Z. Ye *et al.* (HERMES Coll.), hep-ex/0606061.
- [54] M. Mazouz *et al.* (JLab Hall-A Coll.), Phys. Rev. Lett. **99** (2007) 242501.